Subthreshold oscillations and gamma rhythms in the olfactory bulb: a modeling study

Jorge N. Brea [*], **Leslie M. Kay** [† ‡], **and Nancy J. Kopell** [* † §].

[*]Center for BioDynamics, Boston University, Boston, MA,[†]Institute for Mind and Biology, The University of Chicago, Chicago, IL,[‡]Department of Psychology, The University of Chicago, Chicago, IL., and [§]Department of Mathematics and Statistics, Boston University, Boston, MA.

Submitted to Proceedings of the National Academy of Sciences of the United States of America

Gamma oscillations in the olfactory bulb can be produced as an interaction of subthreshold oscillations (STOs) in the mitral cells with inhibitory granule cells. The mechanism does not require that the granule cells spike and we work in a regime in which the mitral cells fire at rates lower than the fast gamma rhythm they create. The frequency of the network is that of the STOs. This allows the gamma to be modulated in amplitude with only small changes in frequency. Gamma oscillations could also be obtained with spiking granule cells, but only for granule cells firing close to population rate.

Mitral cell | Granule cell | Graded inhibition

Abbreviations: MC, mitral cell; GC, granule cell; GCD, granule cell dendrite; GCS, granule cell soma; sLFP, spiking model local field potential; nsLFP, non spiking model local field

Gamma oscillations (40-100 Hz) are produced in the mammalian olfactory bulb (OB) and many other structures in the nervous system [1, 2, 3]. In the neocortex and the hippocampus, gamma oscillations are believed to be dependent on fast-spiking interneurons, created either by the interaction of inhibitory cells alone, or as an interaction of excitatory pyramidal cells and inhibitory interneurons, such as basket cells [4, 5]. It is generally accepted that interactions between excitatory mitral cells and inhibitory granule cells at the dendrodendritic reciprocal synapse support gamma oscillations in the OB, but the physiological mechanisms of these oscillations are not well understood. Many slice studies focus on regimes in which the axonless granule cells spike. However, it has been suggested, by contrast, that gamma oscillations in the olfactory bulb depend on the subtheshold oscillations (STOs) in mitral cells (MCs), the excitatory cells of the OB [6], and that spikes from the granule cells (GCs), the inhibitory cells of the OB, may not play a major part in the gamma oscillation of the OB ([7]; see also Discussion). It is not understood what differences these features might make in the mechanism of synchronization of the OB gamma rhythm.

It is well known that a target population of cells can be synchronized by a common pulse of inhibition [8, 9, 5]. The synchronization comes mainly from a shared suppression of firing until the inhibition has worn off sufficiently for the excitatory cells to fire. If the target cells are identical in drive, they will fire simultaneously; if they have somewhat different drives, they will fire with a small lag [5]. With graded inhibition, it is less clear how the inhibition provides the synchronization. For one thing, there is no clear decay time of inhibition, as the amplitude and time course of the inhibition is not stereotyped.

In this paper, we show that the features of subthreshold oscillations and graded inhibition can work together to produce a new mechanism for the synchronization of gamma. We are interested in the regime in which mitral cells (MCs), the excitatory cells of the OB, spike sparsely (i.e., with a firing rate significantly below that of the population frequency), as seen experimentally [10]. Unlike the classical excitation-inhibition of the pyramidal interneuron network gamma (PING), in which the decay time of $GABA_A$-mediated inhibition is the most important time constant, subthreshold oscillations provide another time constant; in our hands, that is the most important mechanism for determining the population rhythm. The graded inhibition acts to synchronize the STOs and does not synchronize the spikes of the MCs, which are roughly locked to particular phases of the STOs, and do not occur on every STO cycle. The graded inhibition is determined by the activity of the population MC spiking, which then feeds back inhibition at times related to the STO activity. We show that autonomous periodic forcing of the STOs can act like this feedback, even for MCs that are deprived of spiking currents. Forcing by Gaussian noise does not synchronize STOs with different frequencies, nor does forcing by Poisson noise with a related rate. When there are subthreshold oscillations, spiking GCDs can also synchronize the population by synchronizing the subthreshold oscillations without synchronizing the MC spikes. However, in our hands, this occurs only if the GCDs are driven strongly enough to spike at rates approaching that of the population frequency.

Results

Mitral cell population can be synchronized by some kinds of common inhibition. To understand how graded inhibition can produce synchronization, we first deal with a population that has 100 mitral cells but only one granule cell, so the mitral cells get common input. In this work we distinguish graded inhibition from spiking inhibition by two main properties. First, as sketched in Fig. 1A, the activation of graded synapses (-66 mV in our model) occurs below the spiking threshold. Second, while the dynamics of the spiking inhibition depends only on its decay time and the all-or-none threshold, graded inhibition has a soft threshold where the synapse can be partially activated when close to its threshold value; in our model, partial activation is in the range -66.5 to -65.5 mV. (See Supporting Information for graded and spiking synapse equations.) The input to the mitral cells increased substantially and rapidly at 300 ms from its minimum to its maximum in $\sim$50 ms. Fig. 1B contains a raster plot of the MCs when there is no connection to the GCD. In this simulation, the input to the MCs had noise and heterogeneous drive as described in the Methods. Without the connection to the GCD, the natural period of the MC STOs varied between 64 Hz and 72 Hz.

Fig. 1C (left) contains the raster plot of the population of MCs connected to the GCD, showing that the network can produce a population gamma rhythm. Connection to the GCD reduces the firing rate and entrains the STOs to a common frequency. The spikes of the mitral cells do not synchronize (Fig. 1C, right); they fire on different cycles of the population rhythm. However, the subthreshold

Reserved for Publication Footnotes

oscillations do approximately synchronize. The amount of synchronization is quantified by the clustering index (CI) and its coefficient of variation (CV); see Methods. Note that the CI for the simulation of mitral cells with no inhibitory input is above zero (CI = 0.1; CV = 0.54); this is a consequence of the finite time series, with nearby frequencies and finite number of cells. The CI for the system coupled to a single GCD is far greater (CI = .73; CV = 0.2). Note that the successive STOs between MC spikes increase their amplitude. The inhibition associated with GCD input partially resets the initial conditions for the STOs (data not shown). Also note that the power of the sLFP in the inset is significantly larger for Fig. 1C than for Fig. 1B.

The synchronization remains high when the granule cell is replaced by inhibitory input with a periodic alpha function conductance (Fig. 1D). The periodic conductance is modeled on the GCD release of GABA, which occurs during the interval that the GCD voltage is elevated above the threshold for release. In the network, even though the cells receive the same conductance input, they do not receive the same synaptic current, since the post-synaptic voltages are different. To choose the appropriate forcing, we note that Fig. 1D (right) shows the approximately periodic inhibitory conductance produced by the GCD. Using an alpha function with time constant 3 ms for the conductance yields a comparable pulse of inhibition; the size and shape of the forcing is roughly the same as that produced by the internally generated inhibitory conductance.

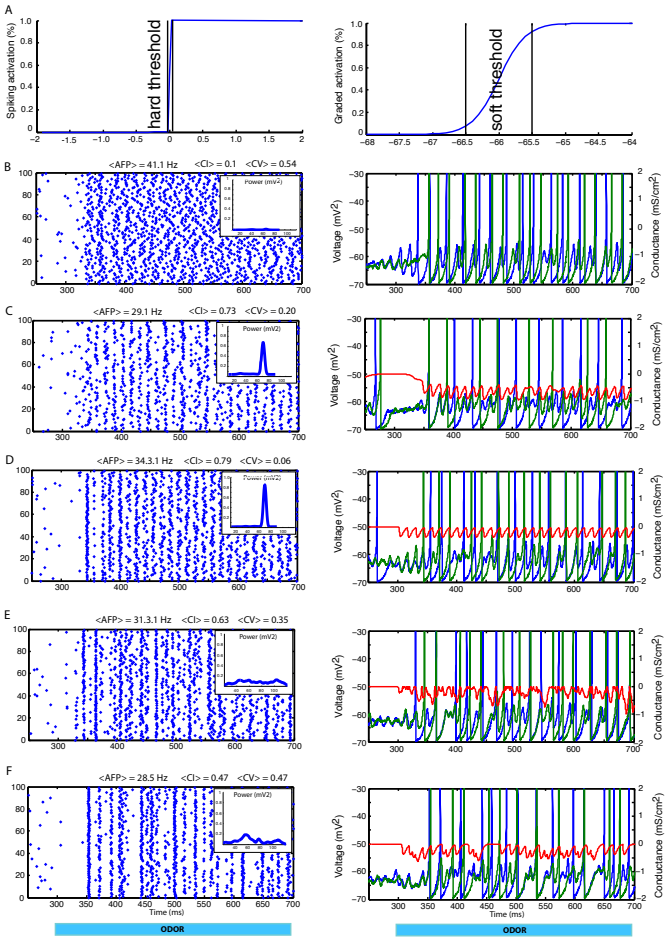

Fig. 1. Uncoupled MCs entrained by common inhibitory periodic input. A. Percentage of open channels as a function of voltage for spiking (left) and graded (right) synaptic conductance. B-F: raster plot of the MC firing (left) showing 450 ms of the 1600 ms simulation. The inset shows the power spectrum, computed during the period of odor stimulation (1000 ms), for the average MC voltages, which we define as our model spiking local field potential (sLFP). Two random MC voltages vs time, with the inhibitory conductance overlaid, are shown on the right. B. Rasterplot for the population of MCs without common inhibition shows no synchronous activity in their firing. Simulated odor is introduced at t = 300 ms. The clustering index (CI) of the MC STOs is low but not zero. Right: Voltage activity of two MCs from the population showing their mixed mode behavior of firing with subthreshold oscillations. C. Raster plot for the MCs coupled to a single GCD. The raster plot after odor input becomes more coherent and the CI increases from 0.10 to 0.73. Voltage activity for two MCs are shown with the synaptic conductance from the GCD (red). The frequency of the inhibitory conductance coincides with that of the gamma rhythm of the MC voltage activity. D. Population of MCs entrained by a periodic alpha function inhibitory stimulation. The raster plot shows rhythmic coherent firing of the MCs. Right:Two MC voltages and the periodic input. E. We replace the periodic alpha function stimulation with random Gaussian noise convolved with an alpha function(red). F. Population of MCs with common Poisson inhibitory input. All MCs receive the same inhibitory input (red) of pulses of alpha function inputs having a Poisson distribution with a rate of $\sim$70 Hz.

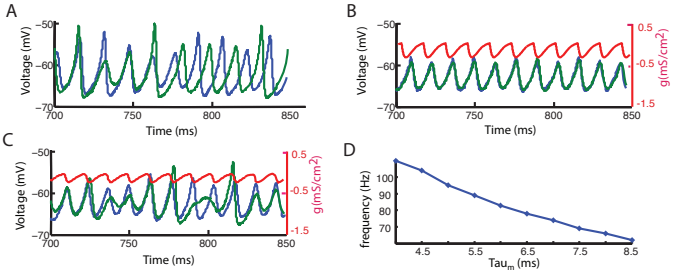

Fig. 2. Periodic input can synchronize STOs. A. Spiking currents are not necessary for sustaining the MC STOs. Voltages for two MCs are shown after removing all intrinsic currents except for the Ks and NaP currents. B. Periodic stimulation strongly synchronizes STOs. The periodic stimulation has the same strength and frequency as in Fig. 1C but the synchronization of the STOs in this case is much stronger. C. Decreasing the strength of the stimulation by half still roughly synchronizes the STOs. D. Frequency of STOs depends on the intrinsic properties of the MCs. Increasing the time constant of the activation variable of the slow potassium current decreases the frequency of the STOs.

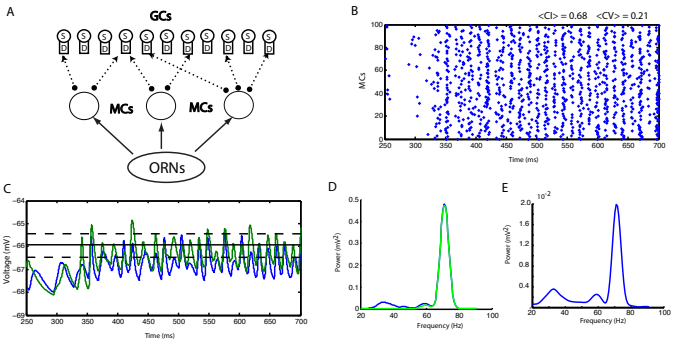

Fig. 3. Sparsely connected population of MCs and GCDs can create fast gamma rhythm with frequency determined by the frequency of the STOs. A. Sketch of the dendro-dendritic interaction between 100 MCs and 1000 GCDs. B. Raster plot showing the spiking activity of the MC population before the odor presentation ($t < 300$ms) and after odor presentation ($t > 300$ms). After odor is presented, population frequency (sLFP and snLFP) has peak at 72 Hz. C. Two representative voltage activity traces for the GCDs in the GCD population. The solid line is the half activation value (-66 mV) of the graded synapse, and the dashed lines represent -66 +/- 0.2 (see Supporting Information). D. Power spectrum for the sLFP (blue) and nsLFP (green) are practically identical. E. Power spectrum for the mean field of the GCD voltage shows that, as a population, the GCD activity oscillates at the same frequency as the MCs (compare with D.)

When the MC firing rate is low, correlated Gaussian noise input to the MCs does not produce a population gamma rhythm (Fig. 1E). Following [11], the Gaussian noise was convolved with an alpha function modeling the effect of synaptic integration. The inhibitory noisy conductance produces sporadic volleys of coherent MC spiking but the sLFP remains incoherent (see power spectrum in the inset of Fig. 1E). The CI is smaller than in panels C and D, but the high CV shows that the measure is not reliable. If the noise is Poisson distributed with a rate close to that of the STOs (λ = Hz) (Fig. 1F), the power spectrum is still broad and the CV large. Thus, in our hands, even if the noise itself has a time constant related to that of the STOs, that is not sufficient for good synchronization. For both Gaussian and Poisson noise, the amplitude of the noise was chosen to produce a conductance of similar intensity as the one given by the $GABA_A$ synapse.

The synchronization of MC STOs does not require spikes in the MCs. Spikes in the MCs are necessary to activate the granule cells. However, as shown in Fig. 1, the granule cells themselves are not critical to the synchronization if the comparable inhibition is provided. Since the MC spikes are not themselves being synchronized and seem necessary only to produce feedback inhibition, the question arises whether the MC spikes play any role other than for the feedback inhibition in synchronization to the STOs. Fig. 2 addresses that question with a pair of MCs.

We first show in Fig. 2A that it is possible to remove the spiking currents of the MCs and retain the STOs. To preserve the approximate amplitude and shape of the STOs we decrease the drive to the MCs compared to Fig. 1. This leads to STOs with amplitudes somewhat larger than those in the full equations for a single MC, but they are still useful to show that spiking currents in the MCs are not necessary for creating the STOs. Fig. 2A shows two uncoupled STOs at about 70 Hz.

In Fig. 2B, we show that the periodic conductance input from Fig. 1C also synchronizes the STOs, even if they are detuned; we chose a detuning of more than 10% in period. With forcing at the same strength and frequency as the inhibition in Fig. 1C, the forcing completely synchronizes the STOs. For forcing of half that size, the synchronization is noticeable but not complete (Fig. 2C). This implies that the current resets that come with MC spiking are not an essential part of the synchronization process. Indeed, the spikes actually make the synchronization more difficult; the same size forcing of the full equations vs the reduced systems leads to only partial synchronization of the STOs in the former. A significant amount of synchronization persists for the full equations even with 30% detuning (see Fig. S1). In Fig S2, we show why the STOs are more difficult to synchronize when the MCs spike. The essential reason is that the STOs do not have constant amplitude between spikes, and are reset between spikes. Since different MCs spike on different cycles of the population rhythm, the correlated input must synchronize heterogeneous STOs in a small time window (two or three STO cycles).

In Fig. 2D we show that the frequency of the STOs can be modulated. To change the STO frequencies, we can either give the MCs different drive or change the intrinsic properties of the currents. Changing the values of the drive also changes the STO amplitude significantly. We therefore chose for Fig. 2D to change the time constant of the activation variable for the Ks current, which is known to change the frequency of the STOs [6, 12, 13]. The STOs depend mainly on the persistent Na and slow K current; thus, the period of the STOs can also be changed by scaling those currents. As is discussed in [12] and [13] the interaction of these two currents display resonant behavior to periodic stimulation. In Fig. S3A we show that for the parameter values used in this work for NaP and Ks, the resonant frequency is very close to the gamma frequency ($\sim$70 Hz). Decreasing the maximal conductance of both these currents decreases the value of the resonant frequency (Fig. S3B)

Synchronization of STOs occurs in a network with multiple granule cells, and determines network frequency. In the previous sections, there was one common inhibitory conductance input for all MCs. The same mechanism still works when the network now contains 1000 granule cells sparsely and randomly connected to the population of 100 MCs as shown in the sketch of Fig. 3A. Each MC connects reciprocally with 20% of the GCDs. The raster plot in Fig. 3B shows that the population can produce a gamma rhythm, with a subset of the mitral cells firing on each cycle. As in Fig. 1, the input to the mitral cells increases from its minimum to maximum value in 50 ms starting at 300 ms. Again, the MC spikes do not synchronize (data not shown). The GCD voltages are correlated, but not fully synchronized; thus the MCs are getting partially correlated input.

The frequency of the population rhythm is that of the STOs. To show this, we compare the sLFP power spectrum (see caption of Fig. 1 for definition) with the power spectrum of the STOs (called nsLFP for non-spiking LFP), to compute the nsLFP we filter out the spikes (see Methods) and calculate the power spectrum of the average of the STOs. Fig. 3D shows that they are almost identical, in power as well as peak frequency. We have also performed this simulation with a set of MCs having significantly lower STO frequencies, by changing the time constant of the activation variable of the Ks current. In that case as well, the population frequency is that of the STO (data not shown). Fig. 3E shows the power spectrum for the mean field of the GCD voltages; note that it has a gamma peak at the same frequency, but with much less intensity. The CI for the fully connected network is lower than that of the network of MCs with only one GC, but larger than the latter receiving Gaussian or Poisson noise and with a lower CV than for the noisy inputs.

As described in the Methods section, the ORN input consists of gaussian noise with an increasing mean as the odor is introduced. It

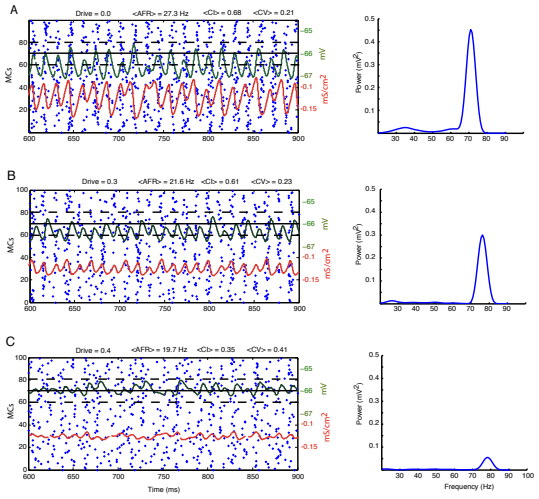

Fig. 4. External constant excitatory drive to GCDs decreases power of the sLFP with only small change in frequency. A. Raster plot (left) and sLFP power (right) show a clear gamma rhythm at ($\sim$70 Hz) for the MC population. The mean field for the GCD subthreshold voltages (green) crosses into and out of the region of graded synaptic activation (black solid and dotted lines). The resultant mean GABAa conductance (red) is also modulated at frequency $\sim$70 Hz (power spectrum not shown). B. Increasing the drive to the GCDs increases the mean depolarization of the GCD voltage, thus increasing the total inhibition to the MCs. The MC spiking rate then decreases but the coherence of their STOs (CI) remains almost unchanged. Therefore the power spectrum of the sLFP remains close to that in A. C. If the GCDs receive too much drive, their voltages remain always above the graded synapse activation threshold and their conductance is almost constant. As a result the MC voltages receive almost constant inhibition incapable of producing a coherent rhythm. This is reflected in the low CI and weak power at the gamma frequency.

can be argued that it is more physiologically realistic to convolve this noise with an alpha function representing synaptic integration. We have not found significant changes in our results when this is taken into account (compare Fig. S4 and 3B).

Additional drive to GCDs changes power without (much) change in frequency. Additional drive to the GCDs mimics added excitatory drive from the piriform cortex and other cortical areas. Increasing drive to the GCDs decreases the sLFP power, but does not much change the frequency (Fig. 4). This is consistent with the idea that the network frequency is given by that of the STOs, which is not changed by drive to the GCDs. What changes much more when the GCD drive is increased is the average firing rate of the MCs and the CI. Note that the CI decreases most between panel B and panel C. The change in drive between those panels is only 0.1, but it has the effect of raising the GCD voltage to a point where the latter is almost always in the regime corresponding to activation of the graded synapse. Thus, the rhythmicity of the inhibitory input to the MCs is decreased. This is consistent with centrifugal inputs to GCDs being one source of desynchronization of the gamma rhythm [14, 15, 16].

Additional drive to MCs changes spiking rate, power and frequency. Additional drive to the MCs mimics increased input from the ORNs. Driving the MCs harder by increasing the mean value of the gaussian ORN inputs (see Methods), increases the spiking rate in the full network, as expected. Less obvious is the effect on sLFP power. The power of the sLFP first increases and then decreases with increased drive (Fig. S5). The differences are associated with changes in the behavior of the GCD population average voltage (as a function of time). As the MCs are driven harder, the GCDs are also driven by the extra firing of the MCs, and their mean voltage over time increases, compare Fig. S5A and S5B. Thus, the graded inhibition is again activated over a larger duty cycle, producing a more uniform conductance forcing. For the largest drive (Fig. S5C), the MCs are not coherent. The increase in MC firing shifts the mean GCD voltage permanently above the graded synaptic activation threshold. The frequency of the network increases with drive, but only by about 10%, as the inhibition also increases with drive to MCs.

It has been shown in experiments that increasing drive to mitral cells can change the frequency of the STOs [6, 12]. There, the MC was isolated, not in a network producing gamma. If we start with a MC whose STO has a frequency of 30 Hz (as in the *in vitro* work), then increasing the drive to that cell can significantly increase the STO frequency (data not shown). To produce a MC with STO frequency in the range of 25-50 Hz, we revert to the scaling of the NaP and Ks maximal conductances used in [12]. Our results are essentially the same as in [12]. Thus, the effect of further drive to a MC can be very different in a single cell than to a cell that is receiving inputs from a population undergoing gamma oscillations.

Sparse spiking inhibition in the granule cells changes frequency of network rhythm. So far, all of the inhibition has been graded inhibition. We now replace the graded inhibition by spiking inhibition to see if that can also produce the gamma rhythm. We also wish to make the spiking of the GCDs sparse [10], and keep the spike rate of the MCs lower than the population rate.

We first change the simulation in Fig. 3 by removing the graded inhibition. This also removes some self-inhibition (see Methods), allowing the GCDs to spike more readily. Fig. 5A shows that this can lead to a new population rhythm in which the MC spikes are crudely synchronized to produce a population rhythm at a much lower rate. This is not due to a larger inhibitory conductance, since lowering the $GABA_A$ maximal conductance did not change the frequency, but made the output less coherent (data not shown). Changing the decay time of inhibition from 18 ms down to 3 ms decreased the period only mildly (from ~ 45 ms to ~ 35 ms). The resulting rhythm is therefore different from PING, in which the time constant of the inhibition has a large effect on the population frequency.

The lack of tight synchronization of the MCs and GCDs is related to the sparseness of the MC to GCD coupling. If connections are made all-all and the decay time is 3 ms, synchronization at gamma is possible, with the MCs firing at population rate (Fig. 5B). This is very much like the PING gamma. The mechanism of this synchronization does not involve STOs (indeed there are no STOs). The all-all connections cause the GCD spikes to fire synchronously, which allows a short effective period of inhibition if the decay time is small enough. In this mechanism, the GCDs fire on every cycle.

Another way to get a gamma population rhythm with GCD spiking is to increase the conductance of the MC to GCD coupling (Fig. 5C). In this case, coupling can be sparse, as in Fig. 3 and Fig. 5A, but the GCDs again fire on almost every cycle. So this parameter range also does not satisfy all the constraints above. In Fig. 5D we show the result of lowering the MC to GCD conductance beyond that of Fig. 5A and adding noise to the GCDs to produce sparse GCD spiking; in this case there is almost no power. Thus, in our hands, it was not possible to produce a gamma oscillation with sparsely spiking GCDs while keeping the MC firing rate lower than the population rate.

Discussion

There is a consensus that dendro-dendritic inhibition plays an important role in synchronization of the mitral cells [7, 17, 18, 19, 20, 21, 22]. However, the mechanisms for this synchronization are still controversial: the granule cells are known to be able to spike and produce graded inhibition, and the roles of these two types of inhibition in synchronization are unknown. Subthreshold oscillations have also been hypothesized to play a role in population oscillations in the OB

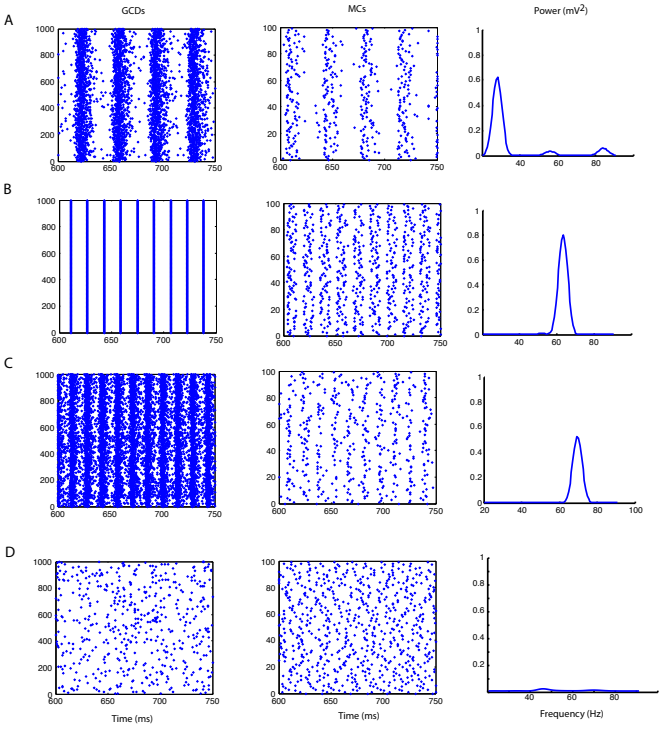

Fig. 5. Gamma rhythm with spiking inhibition. A. Spiking inhibition creates a slow rhythm (30 Hz) for the GCD and MC populations, as shown in rasterplots and power spectrum for the sLFP (right). B. All to all connections between MC and GCDs give rise to a fast gamma if the ORN input to the MCs is strong enough. C. Sparse coupling can also give rise to fast gamma but the GCDs fire in almost every cycle. D. Sparse firing of the GCDs did not give rise to a gamma rhythm.

and elsewhere ([6, 13, 23, 26]), but it has not been previously shown how such subthreshold oscillations could be synchronized

This paper deals with the roles of subthreshold oscillations and different kinds of inhibition (graded and spiking) in the formation of gamma oscillations in the OB. We show that graded inhibition can indeed synchronize mitral cell subthreshold oscillations, and keep them synchronized even in the presence of uncorrelated noise and heterogeneity of inputs to mitral cells. We also show that spiking inhibition can synchronize the STOs, but (in our hands) only when the GCDs spike at high rates comparable to the population rate; reported measurements of spike rates have been much lower [10].

In the model, the time scale for the subthreshold oscillations comes from intrinsic currents of the MCs, notably the slow potassium current and the persistent Na current. The frequency can be increased (or decreased) by making these currents larger (or smaller); it can also be changed by changes in activation time of the Ks current, or drive to the MCs, as shown in the results. Having a range of frequency in the driven STOs is important for the creation of the gamma rhythm when the firing rate is low: it is necessary that some fraction of MCs fire on each cycle to activate the GCs; the noise and the detuning each contribute to the desysnchronization of the MC spiking necessary for this. The STO time scale holds the network at a relatively fixed frequency when the granule cells are driven harder, as occurs when there is feedback from the piriform cortex. This is in sharp contrast to the synchronization mechanism of PING gamma, in which stronger excitation of the inhibitory cells leads to a much lower frequency. The ability of the STO frequency to be changed by modulation of intrinsic currents as well as external drives permits the possibility of different cell assemblies at different frequencies even for comparable drives; this creates a new option for coding of multiple inputs.

The hypothesis that the gamma oscillations do not need granule cell somatic spikes is supported by [7], which showed that if the granule cell somata are removed, the granule cell dendrites, interacting with the mitral cells, still produce gamma. In a preparation that allows granule cell spikes, the latter are not significantly locked to the LFP, suggesting these spikes are not a critical part of the process of producing the oscillations. In this paper, we consider graded inhibition and dendritic spikes. For the former we use a soft threshold for activation of the inhibitory synapse, with $GABA_A$ release dependent on presynaptic voltage in a graded manner.

Graded inhibition can be mediated by AMPA receptors in GC dendrites [30]. This release is associated with voltage-gated calcium channels local to GABA release sites, where NMDA receptor-mediated Ca^{++} influx can be as much as 1 μm away from these sites [30, 31, 32]. Thus, activation of voltage-gated Ca^{++} channels and subsequent release of GABA can be in proportion to depolarization. One issue is whether the dynamics of the Ca^{++} channels near the GABA release sites are sufficiently fast to support gamma oscillations. We do not model this here, but leave this as an important problem for future studies. Another issue is whether depolarization of a spine leading to graded GABA release can spread and influence other MCs not synaptically connected to that spine.

The GCD dendrites are known to have both NMDA and AMPA receptors, with NMDA being prominent in driving GCD excitation [19]. However it has been shown that, after tetanic stimulation or when GCD excitability is increased or when GCD AMPA receptors have increased decay time constants, the AMPA receptors are most responsible for GCD excitation ([34]). We therefore treated the NMDA currents as tonic excitation and did not add this receptor type to the model. There may be several ways of amplifying the excitability of GCDs via neuromodulatory inputs to the EPL, which may underlie enhancement of gamma oscillations in different cognitive circumstances. A recent study showed that cholinergic drive from M1 receptors on GCDs enhances excitability of GCDs and elevates intracellular Ca^{++} [22].

The mechanism for synchronization of the mitral cells by graded inhibition is very different from that of the standard excitation-inhibition interaction that is the basis for the gamma formed by pyramidal cells and proximal fast-spiking interneurons. Unlike the latter, in which the decay time of inhibition is a central parameter [5], in this mechanism the population rhythm is timed by the period of the subthreshold oscillations; changes in drive to the granule cells can change the MC firing rate with only small changes in the population frequency. Indeed, the decay time of the inhibition can be changed by 6 fold, with only $\sim$25% change in period.The uncoupled frequencies of the STOs can detuned, and still have the STOs synchronize, since the granule cell feedback gives correlated (if not common) input to the collection of mitral cells. Hence, the system behaves somewhat as if the STOs are independent oscillators with a common forcing, as in classical theory of forced oscillators; the central difference is that the forcing is itself generated by the mitral cell spikes, which activate the granule cell feedback. However, there is an important difference between the current situation and the classical theory of forced oscillators: as described above and in Fig. S2, when the mitral cells spike, the subthreshold oscillations are not steady, making STO synchronization harder. The STOs also have to synchronize quickly (before the next spike), in contrast to weakly coupled oscillators [24] which allow synchronization over a large number of cycles. In the limit of very sparse spiking of the MCs, the mechanism is close to that of standard coupled oscillators, but at spiking rates seen experimentally, that limit might not be appropriate. A closer approximation for the mitral cells might be "resonate and fire" neurons [25], for which there is not yet a theory of synchronization. Such a theory is beyond the scope of this paper, but might be facilitated by the work that has been done on mixed-mode oscillations [26, 27, 28, 29].

Spiking of the granule cells, when it occurs, is believed to be sparse. We asked if it is possible to produce a gamma rhythm with sparse firing of the GCDs ($\sim$5 Hz) [10]. If the inhibition is strictly through spiking synapses, and the connections from MCs to GCDs are sparse, the behavior of the network depends on the maximal conductance of the excitation from the MCs to the GCDs. When the conductance is large enough, it is possible to get a gamma rhythm in which the MCs spike sparsely and the STOs are synchronized. However, in the parameter ranges we used, this led to spiking of the GCDs at rates comparable to the population frequency, in contrast to reports from the literature [10]. That behavior is similar to persistent gamma produced in neocortex or hippocampus *in vitro* in the presence of kainate and/or carbachol [4], in which fast spiking interneurons spike at population rates and the pyramidal cells spike at low rates. Reducing the conductance from the MCs to the GCDs also did not produce a gamma rhythm with sparse GCD firing: instead, the population produced a slower rhythm in which the GCDs fired at almost every cycle. This reduction in frequency was related to the spread of the spike times of the GCDs: even with a short inhibitory decay time, the inhibition was sufficiently spread out that it was longer than a STO period in these simulations. The spread of the GCDs is related to the lower conductance of the MC to GCD connection: it requires more MCs to spike to get a GCD to spike, and hence this is not immediately induced after some of the MCs start spiking. If the GCDs are forced to be synchronous (e.g., by using all-all coupling instead of sparse coupling), and the mitral cells are driven very hard, then there is a gamma rhythm with GCDs again firing on every cycle.

Other models of OB synchronization use different hypotheses. The Bathelier et al. model [12], which produced a gamma rhythm, did not contain physiological granule cells; instead, mitral cell spiking led to self and lateral inhibition. Hence, the fictive granule cells are essentially spiking on every cycle. The Davidson et al. model [35] has detailed biophysical descriptions of both MCs and GCs, with GCDs spiking, but the rhythm produced by that model is, like Fig. 5A in the current paper, lower than the gamma frequency. In [34]. Schoppa showed experimentally that MCs can be partially synchronized if they get synchronized IPSPs; however, our models suggest that, if the MC to GCD connections are sparse and the inhibition is from spiking GCDs, the IPSPs will not be synchronous. In another

biophysical model of synchronization of MCs and GCDs, David et. al. [36] showed that recurrent inhibition to an initially disorganized MC population could increase the variance of the MC spike timing, suggesting that that sniffing or other early mechanisms of temporal coordination might be important. However, the gamma oscillations we are describing ([37]) occur during fast sniffing, when MC spiking is decoupled from sniffing [2]. Thus, the situation does not allow a resynchronization with each sniff.

With graded inhibition in our model, correlated noise has a different effect than in that of Galan et. al. [11]. One major difference in the models is that, in Galan et al. the MCs fire at approximately the same rate as the population frequency, about 25 Hz. In our models the firing rate is about the same, but the sLFP frequency is much higher as in [37]. With Gaussian or Poisson inputs at the same rate as the firing rate, [11] produced synchronization of the MC spikes and therefore the population. In our model, neither produces the synchronization of the STOs (or the population).

In summary, this work proposes a new mechanism for the creation of gamma oscillations in the OB, making use of both subthreshold oscillations in the MCs and graded inhibition from the GCDs. This rhythm differs from both the PING rhythm and persistent gamma in neocortical and hippocampal slices. We also suggest that, with sparse connections and the biophysical properties of GCDs and MCs in the current literature, sparsely spiking GCD synapses (spike rates significantly lower than the sLFP frequency) cannot produce gamma oscillation at the frequencies seen in [37]. The model makes predictions about properties of graded inhibition and suggests new computational functionality for the OB gamma rhythm.

Methods

The models in this paper are biophysically based but use a small number of compartments. The OB was modeled using 100 mitral cells (MCs) and 1000 granule cells (GCs). Each MC represents the activity of a single glomerulus; MCs innervating the same glomerulus are assumed synchronous [33]. A schematic of the model is shown in Fig. 3A. The MCs are single compartment models with fast transient and persistent sodium currents, a delayed rectifier and two transient potassium currents and , with details from [12]. In [12], the frequency of the STOs was chosen to be in the range 25-50Hz corresponding to the frequency range observed *in vitro* [6]; we modified some parameters to make the STO frequency faster, in the range of the gamma frequency observed *in vivo* 60-90Hz [37]. To do this we increased the maximal conductances of the NaP and Ks currents; although this is faster than the STOs seen *in vitro*, rhythms *in vivo* are often faster than those *in vitro*; indeed, the OB gamma is faster *in vivo* than *in vitro* [6, 7, 37], and the *in vitro* gamma is also about the same frequency as the *in vitro* STOs. The periods of the STOs are determined by both intrinsic currents and external drive, and the periods within each simulation are chosen to be over a range of values of about 10%. (See also Fig. S1.) In some of the simulations, this detuning comes only from differences in drive, while in others there are also differences in intrinsic currents.

Each MC received independent excitatory input from olfactory receptor neurons modeled as a noisy input with rising baseline modeling the introduction of the odor. GCs were modeled with two compartments, a dendrite (GCD) and a soma (GCS). The soma was given fast sodium and delayed rectifier potassium currents, and M-type and A-type potassium currents. The dendrite was given the same currents as the soma, except for the M-type and A-type currents. Details are from [35, 38]. Since the interaction between the MCs and GCDs is dendro-dendritic, the GCS serves only as a load to the GCD. A more explicit and dynamic role for the GCS becomes evident when other parts of the olfactory system are involved (e.g, the piriform cortex); these do not play a significant role in this work but are important for future models (unpublished). ORN activity was represented as a noisy gaussian to the mitral cells, changes in ORN drive are modeled by changes in mean of gaussian input (see Supplementary Information for equations). GCD dendrites were randomly connected to the MCs via reciprocal dendrodendritic synapses with a probability of 0.2.

GCDs receive excitatory input with AMPA kinetics (see discussions for why NMDA receptors were not considered). In all simulations GABA release can be due to either spikes (spiking inhibition) or subthreshold depolarization (graded inhibition). For both kinds of synapses the form of the equation for synaptic release is governed by the rise time and decay time. There are differences in the literature about the length of the inhibitory decay time [34, 35]. Because of this we have used decay times of both 18ms and 3ms; there was almost no change in our results. The difference between graded and spiking inhibition is given by the shape of the activation function (sigmoid), whose midpoint sets the activation threshold, and whose slope at that point determines the degree of gradation in dependence of release on voltage (see Supporting Information.)

To study the coherence of the MC STOs we filtered the spikes from the MC voltage activity. We used the MATLAB function fir1 to band pass filter the signals from 50-90 Hz and then used the MATLAB function filtfilt to avoid phase shifts of the signal. This allowed us to approximately preserve the STO structure of the MC voltages while filtering their spikes. To estimate the phase coherence of the MC STOs, we measured the order parameter C(t) as given in the Supporting Information. The clustering index (CI) was defined as the time average of C(t) during odor stimulation (300-1300 ms). The coefficient of variation of C(t) (CV = σ(C(t))/mean(C(t))) was also calculated for the same time window corresponding to odor stimulation. The power spectra for the sLFP and snLFP were calculated over one second period during odor stimulation. Each time series is subdivided into three time windows with 50% overlap. All measures were averaged over five trials.

ACKNOWLEDGMENTS. All authors were supported by the NIDCD R01-DC007995 CRCNS program.

1. **Balu R, Larimer P, Strowbridge BW (2004) *J Neurophysiol* 92: 743–53.**
2. **Kay LM, Laurent G (1999) *Nat Neurosci.* 2: 1003–9.**
3. **Rinberg D, Koulakov A, Gelperin A (2006) *J Neurosci.* 26: 8857–65.**
4. **Whittington MA, Traub RD, Kopell N, Ermentrout B, Buhl EH (2000) *International journal of psychophysiology : official journal of the International Organization of Psychophysiology* 38: 315–36.**
5. **Börgers C, Kopell N (2003) *Neural computation* 15: 509–38.**
6. **Desmaisons D, Vincent JD, Lledo PM (1999) *J Neurosci.* 19: 10727–37.**
7. **Lagier S, Carleton A, Lledo PM (2004) *J Neurosci* 24: 4382–92.**
8. **Börgers C, Epstein S, Kopell NJ (2005) *Proc Natl Acad Sci* USA 102: 7002–7.**
9. **Börgers C, Epstein S, Kopell NJ (2008) *Proc Natl Acad Sci* USA 105: 18023–8.**
10. **Cang J, Isaacson JS (2003) *J Neurosci.* 23: 4108–16.**
11. **Galan, Fourcaud-Trocme N, Ermentrout G, Urban N (2006) *Journal of Neurosci.***
12. **Bathellier B, Lagier S, Faure P, Lledo PM (2006) *J Neurophysiol* 95: 2678–91.**
13. **Hutcheon B, Yarom Y (2000). *Resonance, oscillation and the intrinsic frequency preferences of neurons.***
14. **Gray CM, Skinner JE (1988) *Experimental brain research Experimentelle Hirnforschung Expérimentation cérébrale* 69: 378–86.**
15. **Kay L M, Freeman W J (1998) *Behav Neurosci.* 112(3): 541-553.**
16. **Nusser Z, Kay L M, Laurent G, Homanics G E, Mody I (2001) *J Neurophysiol.* 86(6): 2823-2833.**
17. **Schoppa NE, Urban NN (2003) *Trends Neurosci. 26: 501–6.***
18. **Schoppa NE, Westbrook GL (1999) *Nat Neurosci.* 2: 1106–13.**
19. **Schoppa N, Kinzie J, Sahara Y, Segerson T (1998) *J Neurosci.***
20. **Luna VM, Schoppa NE (2008) *J Neurosci* 28: 8851–9.**
21. **Isaacson JS, Strowbridge BW (1998) *Neuron* 20: 749–61.**
22. **Balu R, Pressler RT, Strowbridge BW (2007) *J Neurosci* 27: 5621–32.**
23. **Chorev E, Yarom Y, Lampl I (2007) *J Neurosci.* 27: 5043–52.**
24. **Kopell N. J., Ermentrout G. B. (2002) *Handbook of Dynamical Systems Volume 2, North Holand* pp 5-54**
25. **Izhikevich E. M. (2001) *Neural Networks* Volume 14, Issues 6-7, pp 883-894**

26. Rotstein H. G., Oppermann T., White J. A., Kopell N. J. (2006) *Journal of computational neuroscience* 21(3) pp. 271-92
27. Brons M., Kaper T. J., Rotstein H. G. (2008) *Chaos* vol. 18 (1) pp. 015101
28. Yu N., Kuske R., Xian Li Y. (2008) *CHAOS* vol. 18, 015112
29. Drover J., Rubin J., SU J., Ermentrout B. *SIAM J. APPL. MATH.* Vol. 65, No. 1, pp 69-92
30. Isaacson J S (2001) *Proc Natl Acad Sci* USA 98: 337–42.
31. Sassoè-Pognetto M, Ottersen OP (2000) *J Neurosci.* 20: 2192–201.
32. Price JL, Powell TP (1970) *J Cell Sci.* 7: 125–55.
33. Schoppa N. E., Westbrook G. L., (2001) *Neuron* 31: 639 — 651.
34. Schoppa N. E. (2006) *Neuron* 49: 271–83.
35. Davison AP, Feng J, Brown D (2003) *J Neurophysiol* 90: 1921–35.
36. David F, Linster C, Cleland TA (2008) *Journal of computational neuroscience* 25: 25–38.
37. Beshel J, Kopell N, Kay LM (2007) *J Neurosci.* 27: 8358–65.
38. Bhalla US, Bower JM (1993) *J Neurophysiol* 69: 1948–65.

Supporting Information

Cell equations

Mitral cells and granule cells are implemented as conduction based models following Hodgkin-Huxley kinetics. Mitral cells are modeled using a single compartment. Except for the maximal conductance for the slow potassium (K_s) and persistent sodium Na_P currents, as well as the time constant for the activation variable for K_s, all equations and parameters for the mitral cells are taken from [12]. Granule cells have a somatic and a dendritic compartment, with equations and parameter values taken from [35, 38]. The membrane capacitance for all cells is $1\mu F/cm^2$ and therefore not mentioned explicity in the voltage equations. The following units where used: Conductance per unit area in $[mS]/[cm^2]$, current per unit area in $[\mu A/cm^2]$, voltage in $[mV]$ and time (t) in [ms]. The kinetic equations for all cell compartments k have the form:

$$\dot{v_k} = -I_L - \sum_i I_i - \sum_s I_s + \sum_e I_e + \sum_j g_{k,j}(v_j - v_k) \quad \textbf{[1]}$$

where I_L , I_i, I_s, and I_e are the leak, ionic, synaptic and external currents respectively. $g_{k,j}$, v_i, and v_j represent the electrotonic conductance and voltages between adjacent compartments k and j in a given cell. The leak current is governed by the linear ohmic equation $I_L = g_L(v - E_L)$ with g_L the leak conductance and E_L its reversal potential. For mitral cells g_L = 0.0, for the granule cell soma and dendrite g_L = 0.0083. For both mitral cells and granule cells the reversal potential is set to E_L = -65.

The mitral cells have two sodium currents I_{Na}, I_{NaP} and three potassium currents: I_{Kfast}, I_{K_A} and I_{K_s}. The granule cell soma has one sodium current I_{Na} and three potassium currents: I_K, I_{K_A} and I_{K_M}. The granule cell dendrites have a sodium current I_{Na} and a potassium current I_K. All these currents are described by the equation:

$$I_i = g_i m^M h^H (v - E_i) \quad \textbf{[2]}$$

where g_i is the maximal conductance and E_i the reversal potential. The activation and inactivation variable m and h raised to the power M and H respectively follow the kinetic equations:

$$\dot{m} = (m - m_\infty(v))/\tau_m(v) \quad \textbf{[3]}$$

$$\dot{h} = (h - h_\infty(v))/\tau_h(v) \quad \textbf{[4]}$$

The functional form of the stationary states m_∞, h_∞ and the characteristic time constants τ_m, and τ_h are not the same for all currents. For the current I_{Kfast} in the mitral cell and the currents I_{Na} and I_K in the granule cell dendrite and soma, we used values taken from Senselab databank (http://senselab.med.yale.edu) adapted from (Ballah and Bower 1993). For the mitral cell curents I_{K_A} and I_{K_s} and the granule cell somatic and dendritic current I_{K_A} the functional form is given by:

$$m_\infty, h_\infty = \frac{1}{exp[-(v - v_0)/\sigma_0] + 1} \quad \textbf{[5]}$$

$$\tau_{m,h} = \tau_0 + \frac{Aexp[-(v - v_1)/\sigma_1]}{exp[-(v - v_2)/\sigma_2] + 1} \quad \textbf{[6]}$$

Both m_∞ and h_∞ are defined by the pair of parameters (v_0, σ_0) specifying the half value (v_0) and the steepness of the sigmoid at the half value (σ_0). The time constants τ_m and τ_h are defined by the set of parameters $(\tau_0, A, v_1, \sigma_1, v_2, \sigma_2)$. Values for these parameters and the maximal conductance g are given in the table below. For these currents M = 1, H = 1 and E = -70. Note: if the exponential in the numerator or denomenator of equation 6 is set to 1, $v1$ and σ_1 are given by a dashed line.

	g	$v_{0,m}$	$\sigma_{0,m}$	$\tau_{0,m}$	A_m	$v_{1,m}$	$\sigma_{1,m}$	$v_{2,m}$	$\sigma_{2,m}$	$v_{0,h}$	$\sigma_{0,h}$	$\tau_{0,h}$	A_h	$v_{1,h}$	$\sigma_{1,h}$	$v_{2,h}$	$\sigma_{2,h}$
K_s (MC)	150	-34	6.5	7	0	-	-	-	-	-65	6.6	20	22	-	-	-71.6	6.85
K_A (MC)	10	70	14	0	25	-45	13.3	-45	10	-47.4	6	0	55.5	-70	5.1	-70	5
K_A (GCS)	8.8	-42	13	1.38	0	-	-	-	-	-110	18	150	0	-	-	-	-

The equations describing the I_{KM} current at the granule cell soma are as follows:

$$m_\infty = \frac{1}{exp[-(v + 35))/5] + 1} \quad \textbf{[7]}$$

$$\tau_m = \frac{1000}{[exp[-(v + 35)/40 + exp(-(v + 35)/20]} \quad \textbf{[8]}$$

where g_{K_M} = 133.4, M = 3, H = 0 and E_{K_s} = -70.

The I_{NaP} current in the mitral cell has no inactivating variable and the time scale for the activation variable m is fast enough to consider $m(v) = m_\infty$. Therefore the NaP currents has the simplified form $I_{NaP} = 0.7(1/(exp(-(v+51)/5)+1))(v-45)$. The mitral cell I_{Na} rate functions are described by the following rate equations:

$$a_m = 0.32(V+50)/\{1-exp[-(V+50)/4]\} \quad \textbf{[9]}$$

$$b_m = 0.28(V+23)/\{exp[(V+50)/5]-1\} \quad \textbf{[10]}$$

$$a_h = 0.128/exp[(V+46)/18] \quad \textbf{[11]}$$

$$a_m = 4/\{1+exp[-(V+23)/4]\} \quad \textbf{[12]}$$

$with$

$$m_\infty = a_m/(a_m+b_m) \quad \textbf{[13]}$$
$$h_\infty = a_h/(a_h+b_h) \quad \textbf{[14]}$$
$$\tau_m = 1/(a_m+b_m) \quad \textbf{[15]}$$
$$\tau_h = 1/(a_h+b_h) \quad \textbf{[16]}$$

and g_{Na} = 10, M = 3, H = 1 and E_{Na} = 45.

Synaptic equations

The olfactory bulb model has two type of synapses, graded and spiking synapses. Spiking synapses can be either excitatory (AMPA) or inhibitory ($GABA_A$). In all cases their dynamics are described by:

$$I_s = gs(V_{post} - E) \quad \textbf{[17]}$$

$$\dot{s} = \alpha(1-s)T - \beta s \quad \textbf{[18]}$$

$$T = \frac{1}{exp[-(v-v_3)/\sigma_3]+1} \quad \textbf{[19]}$$

where g is the maximal conductance, V_{post} the post synaptic voltage, s the normalized conductance and E the reversal potential. For excitatory synapses (AMPA) E = 0, for inhibitory synapses ($GABA_A$) E = -70. The percentage of open channels is governed by the sigmoidal function T; it defines whether the synapse kinetics is graded or spiking. In this work the graded $GABA_A$ synapse was centered at v_3 = -66, and the gradedness of the release was set by σ_3 = 0.2. For the spiking synapse, v_3 is set to 0 and σ_3 = 0.01.

External currents

The external currents I_e can represent the ORN input to the MCs or any other input to the MCs or the GCs. In this work they followed the general functional form:

$$I_e = f(t) + D\psi(t) \quad \textbf{[20]}$$

$f(t)$ is a given deterministic function and $\psi(t)$ represent white Gaussian distributed noise with standard deviation D. The activation of ORN input was modeled using the sigmoidal function:

$$f(t) = f_0 + \frac{1}{2}(f_1 - f_0)[(tanh((t-t_{orn})/(r/3)-3)+1] \quad \textbf{[21]}$$

Where f_0 is the pre-odor value, f_1 the stationary odor value, r sets the rate of increase from f_0 to f_1 and t_{orn} the time of odor onset. The ORN input to each MC is defined by the parameters D from equation 20 and f_0, f_1 and r from equation 20. The MCs receive independent input. The distribution of values for f_0, f_1 defines the degree of heterogeneity of the preodor and odor periods. These values were taken from a uniform distribution with bounded range. The range was taken as a percentage (30%) of the mean value so $f_0 \in (0.2, 0.4)$ and $f_1 \in (2.1, 3.9)$. In all simulations D = 0.2.

Model LFP, power spectra and clustering index

All analyses were done using MATLAB 7.5 software by MathWorks, Inc. The statistical analyses (power spectra and clustering index) were performed over a 1000 ms windows corresponding to the odor stimulation time (300 - 1300 ms).

In this work we modeled the LFP of a population from the mean field of the MC voltages. We defined the spiking local field potential (sLFP) as the mean value of the complete MC signal (spikes included); we would get a different measure from using synaptic currents or voltages of the GCD cells, but the periodicity would be the same, and all such measures are related to degree of synchrony of the network. The non-spiking local field potential (nsLFP) was defined as the mean values of the MC voltages after filtering the each signal from 50-90 Hz leaving only the STOs as the main component of each signal. To filter these signals we used a two way filter using the MATLAB functions FIR1 and FILTFILT. Modeled LFP were band pass filtered from 10-120 Hz. Power spectrums for each signal are computed using the MATLAB function PWELCH with 50% overlap. All measures where tested over 5 trials. The clustering index (CI) used to measure phase coherence of the STOs in the MC was obtained by first extracting the phase the nsLFP signals. This was accomplished using the Hilbert transform on the nsLFP. An order parameters can then be define as shown below.

$$C(t) = \frac{1}{N}|\sum_{k=1}^{N}\exp(i\phi_k(t))| \qquad \textbf{[22]}$$

where N is the number of mitral cells. We define CI as the time average of C(t) ($\widehat{C(t)}$). We then calculate the averaged CI (<CI>) over five trials. We also measured the coefficient of variation of C(t) as CV = $\sigma(C(t))/\widehat{C(t)}$ were σ is the standard deviation. CV was also averaged over the same five trail (<CV>).

Supporting figures

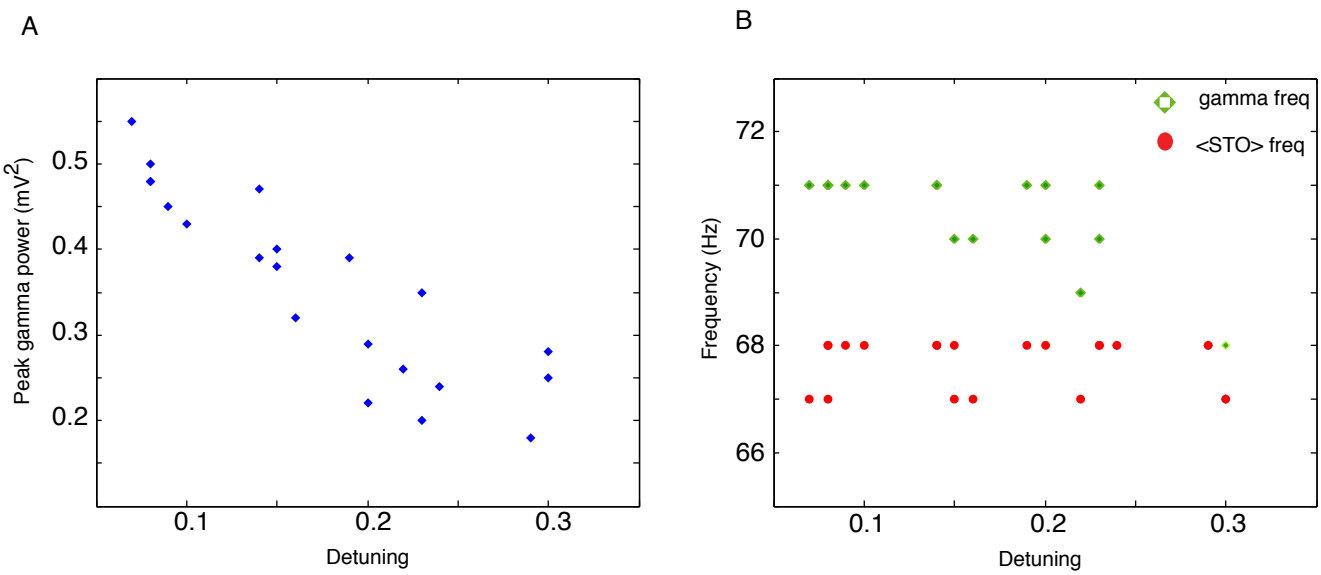

Fig. S1 Gamma power persists with strong frequency detuning. A. Scatter plot showing that increased detuning of the STO frequencies decreases the gamma power but the latter is still significantly high even for strong detuning. The detuning is measured as the difference between the maximum and minimum STO frequencies in the uncoupled network, normalized by the mean STO frequency from the whole MC population. The detuning is computed for each run (one point) over a 1000 ms window before the MCs interact with the GCDs. The MCs and GCDs are connected together to get a gamma rhythm for which the power is calculated. B. The mean frequency of the gamma power plotted in A (green) decreases with increased detuning and becomes more variable. The mean frequency of the uncoupled STOs remains almost constant (red). (The frequency resolution for this analysis is 1Hz.) Note that the mean frequency of the uncoupled STOs is lower than the peak frequency of the coupled network.

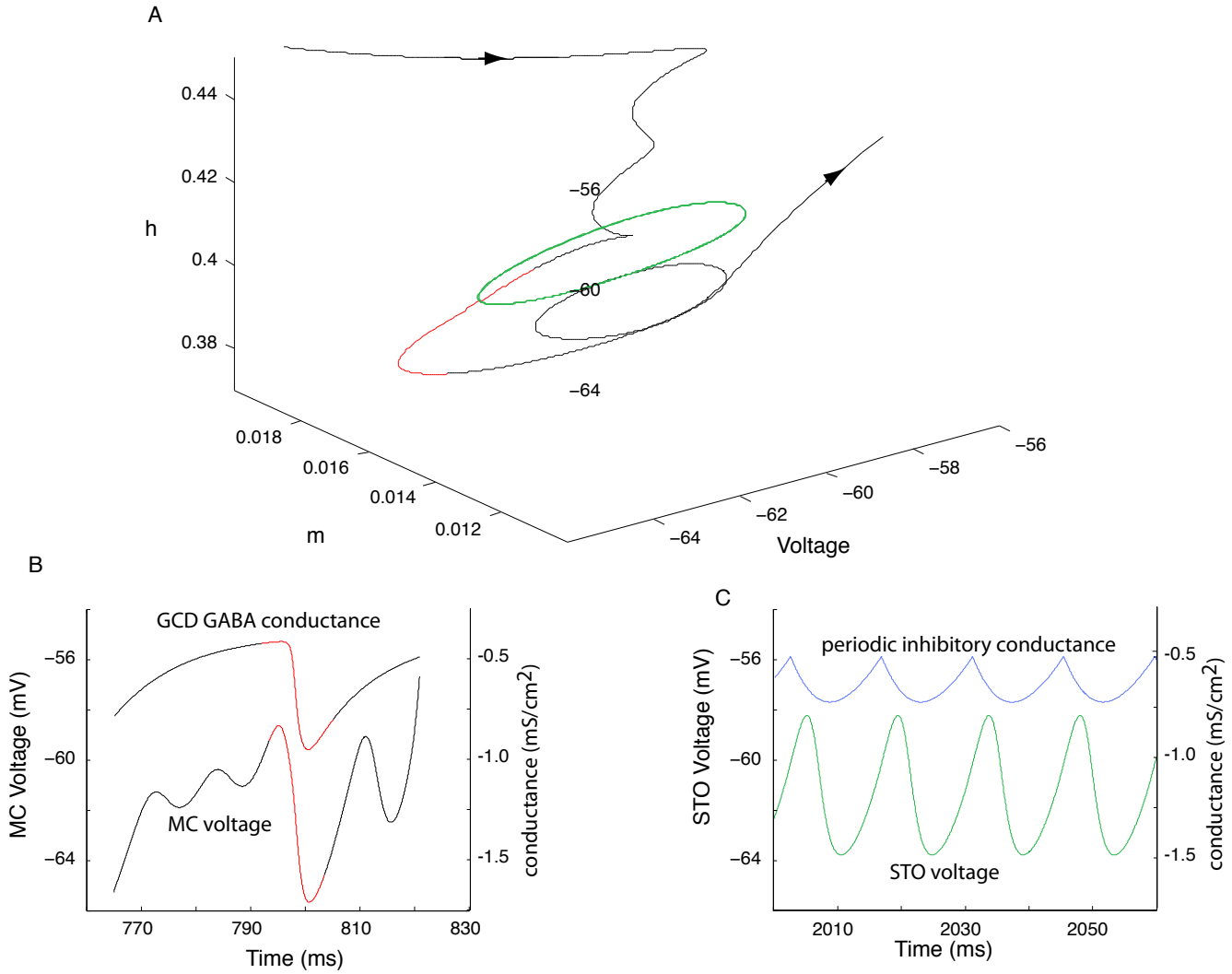

Fig. S2 Interspike MC STOs dynamics is not the same as the dynamics given by the MCs without the spiking currents. A. Since K_s and Na_P are the predominant currents during the STOs, the phase space of a MC can be reduced to three dimensions given by the activation (m) and inactivation (h) state variables for K_s and the MC voltage. The black and red trace shows the STO dynamics in between two spikes. The red section of the trajectory indicates the portion during resetting by the inhibitory granule cell. The green trace shows the dynamics of the STOs when the spiking currents have been removed. B. Top: the stimulation from the GCD to a MC. Bottom: the effect of this inhibition on the MC. C. Top: periodic inhibition to the green trace in A. Bottom: effect of that inhibition on the MC. Comparing B. and C we see that the STOs for the non-spiking MC are steady, while the STOs for the spiking MC increase in amplitude and reset with the spike.

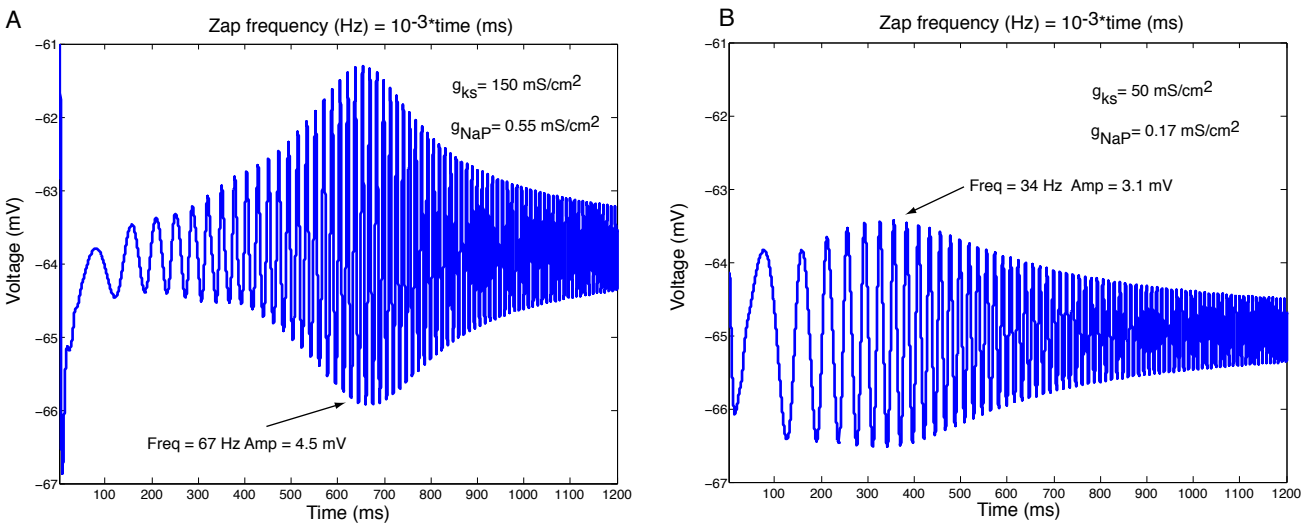

Fig. S3 MC STOs exhibit a resonant frequency under periodic stimulation. A. A zap current with frequency changing linearly in time is applied with subthreshold intensity to a MC. In this subthreshold regime the predominant currents defining the MC voltage dynamics is given by the slow potasium current K_s and the persistent sodium currents Na_P. The resonant frequency for the MC STOs depends on the parameters of these two currents (e.g., their maximal conductance and the activation time constant for Ks). For the parameters used to get gamma oscillations in the modeled OB, the resonant frequency 67 Hz is very close to the frequency of the gamma rhythm of the model. B. Changing the the maximal conductance of K_s and Na_P can change the resonant frequency significantly.

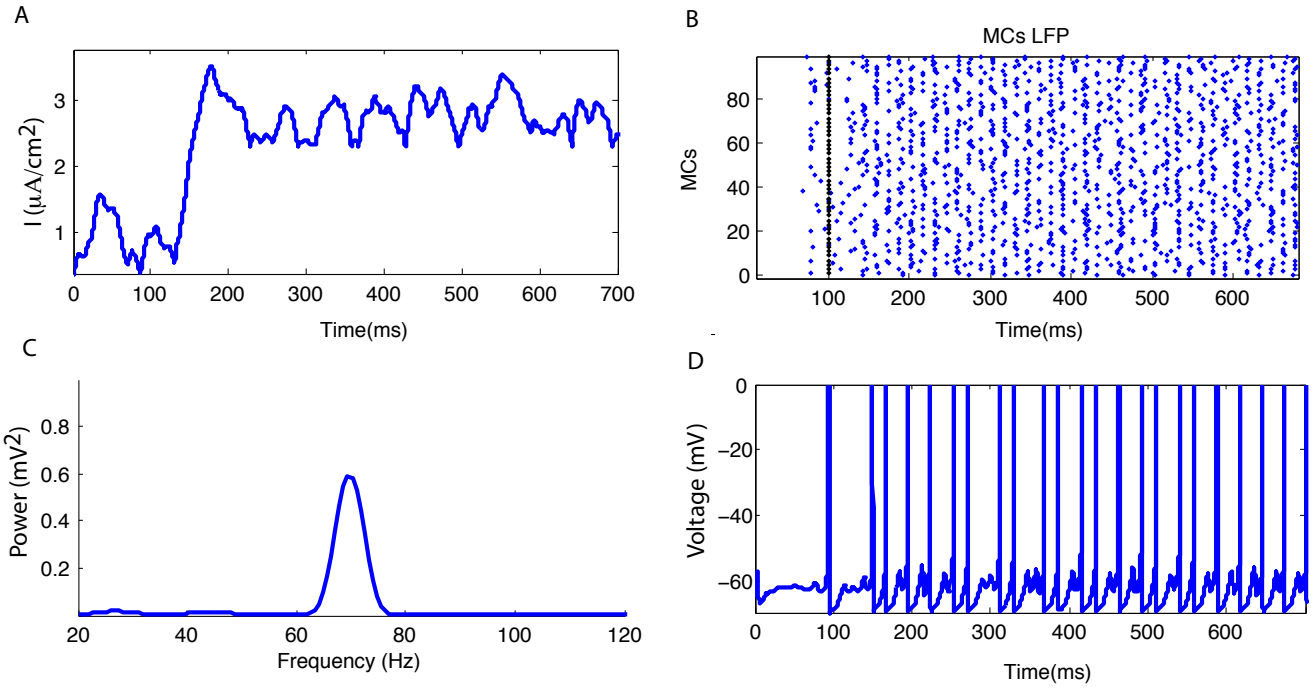

Fig. S4 Fast gamma rhythm persists when gaussian noise from ORN inputs is convolved with an alpha function. A. ORN input to one of the MCs in the OB population. B. Raster plot of the MC population shows sparse spiking at a fast gamma rhythm as in Fig. 3B. C. Power spectra of the sLFP with a well defined gamma frequency peak at $\sim$70Hz. D. Spike for a single MC in the OB population shows irregular spiking with STOs.

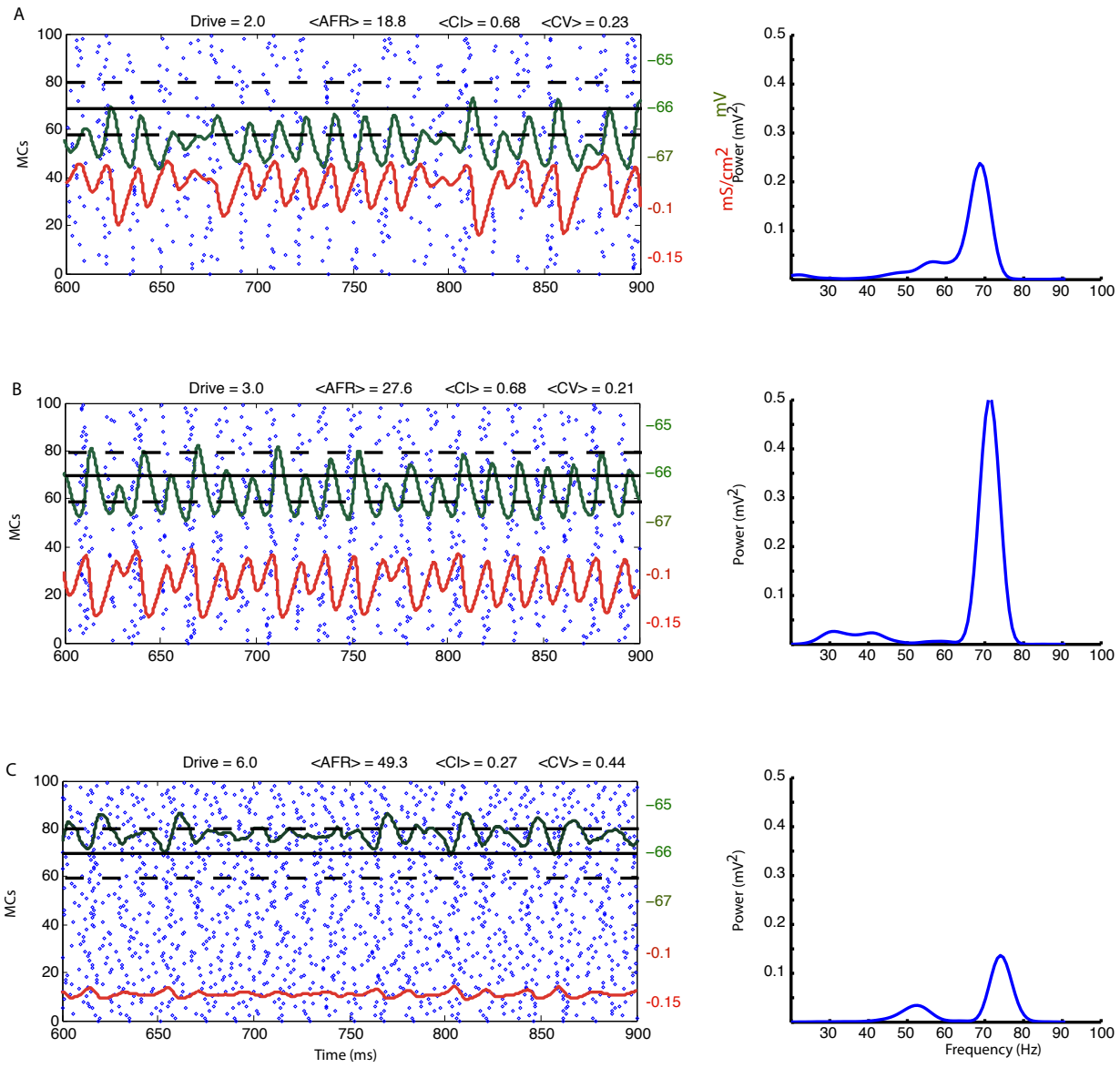

Fig. S5 External constant excitatory drive to MCs changes power of the sLFP, MC spiking rate and frequency. A. Raster plot (left) and sLFP power (right) show a clear gamma rhythm at (∼70 Hz) for the MC population. The mean field for the GCD subthreshold voltages (green) crosses into and out of the region of graded synaptic activation (black solid and dotted lines). The resultant mean $GABA_A$ conductance (red) is also modulated at frequency ∼70 Hz (power spectrum not shown). B. Increasing the drive to the MCs increases the mean depolarization of the GCD voltage, thus increasing the total inhibition to the MCs. The MC spiking rate then decreases but the coherence of their STOs (CI) remains almost unchanged. Therefore the power spectrum of the sLFP remains close to that in A. C. If the MCs receive too much drive, they depolarize the GCDs voltages constantly above the graded synaptic activation threshold and their conductance is almost constant.